Schwinger boson mean-field theory of the kagome Heisenberg antiferromagnet with Dzyaloshinskii-Moriya interactions

Kallol Mondal and Charudatt Kadolkar
Department of Physics, Indian Institute of Technology Guwahati, Guwahati, Assam 781039, India
(Received 26 December 2016; published 4 April 2017)

We have studied the effect of the Dzyaloshinskii-Moriya interaction on kagome Heisenberg antiferromagnet using the Schwinger boson mean field theory (SBMFT). Within SBMFT framework, Messio *et al.* had argued that the ground state of the kagome antiferromagnet is possibly a chiral topological spin liquid [Phys. Rev. Lett. **108**, 207204 (2012)]. Thus, we have computed a zero-temperature ground-state phase diagram considering the time-reversal symmetry breaking states as well as fully symmetric *Ansätze*. We discuss the relevance of these results in experiments and other studies. Finally, we have computed the static and dynamic spin structure factors in relevant phases.

DOI: 10.1103/PhysRevB.95.134404

I. INTRODUCTION

Quantum spin liquids (QSLs) [1] are the exotic states of matter without any broken symmetries even at $T = 0$, the states of matter which cannot be explained in the paradigm of Landau's symmetry-breaking theory [2–5]. The most promising candidate to posses spin liquid ground states is the spin-1/2 kagome Heisenberg antiferromagnet (KHAF) due to its low dimensions, small spin, and strong geometrical frustration [6–9]. One of the challenges of the search for QSL among materials is the presence of anisotropies like Dzyaloshinskii-Moriya (DM) interaction. Such interactions reduce symmetry and quantum fluctuations, and lead to magnetic ordering. The Dzyaloshinskii-Moriya interaction [10,11] arises when there is lack inversion symmetry in the lattice.

The mineral, herbertsmithite, is an example where the spin-1/2 copper atoms form a kagome lattice. No magnetic order has been found down to 50 mK with the exchange coupling being 170 K [12,13]. To explain the spin susceptibility enhancement of herbertsmithite [14] at low temperature, a small value of Dzyaloshinskii-Moriya interaction has to be considered. The presence of DM interaction is also confirmed by paramagnetic resonance [15], where the DM interaction of strength of $0.08J$ is needed to explain the linewidth. Small values of DM interaction can produce long-range order (LRO) in a spin system, especially in spin liquid ground states. So it was not clear why spins do not freeze in herbertsmithite at low temperatures.

The effect of DM interaction on the kagome Heisenberg antiferromagnet has been studied by several groups [16–21]. From exact diagonalization (ED), Cépas *et al.* [18] found that there is a critical point at $D_c = 0.1J$ where there is a moment-free phase at the lower side and Néel phase on the other. This result is consistent with experiments, since estimated DM interaction strength is about $0.08J$ in herbertsmithite. Huh *et al.* has proposed a quantum critical theory [22] about the critical point suggested by Cépas *et al.* [18] Messio *et al.* [21], using Schwinger boson mean-field theory (SBMFT), have calculated the phase diagram and showed that the results are qualitatively similar to the ED studies in the small boson density region.

The purpose of this paper is twofold. In 2013, Messio *et al.* [23] showed that in the SBMFT framework, the ground state of the kagome Heisenberg antiferromagnet is a chiral $\mathbb{Z}_2$ spin liquid. In their study of DM interaction, they had not considered the time-reversal symmetry breaking *Ansätze* [21]. This would change the phase diagram for small strengths of DM interaction. Second, they considered only bond creation mean field $\mathcal{A}$. However, the inclusion of a second boson hopping mean field, a $\mathcal{B}$ field, improves the quantitative agreement of the bandwidth in the excitation spectrum of the Heisenberg model on a triangular lattice [24]. Flint and Coleman showed that these two fields together give a better description of these frustrated systems [25]. Thus, we, in this paper have considered a chiral spin liquid *Ansatz* and also included the hopping mean field.

In Sec. II we present the model and the brief description of Schwinger boson mean field theory with two bond operator's. In Sec. III we describe the detailed algorithm for the numerical search of the optimum points. In Sec. IV we present the zero-temperature ground-state phase diagram with properties associated with it and the effect of DM interaction on the QSL ground state. We discuss the connection between the prediction of our model with experimental results. We have also calculated the dynamical structure factor of the different *Ansätze* in relevant phases in Sec. V.

II. MODEL AND FORMALISM

The Hamiltonian for the nearest-neighbor Heisenberg model with Dzyaloshinskii-Moriya interaction is given by

$$H = \sum_{\langle ij \rangle} [J \vec{S}_i \cdot \vec{S}_j + \vec{D}_{ij} \cdot (\vec{S}_i \times \vec{S}_j)], \tag{1}$$

where $\langle ij \rangle$ stands for a pair of neighboring sites i and j. The pairs are directed due to the DM interaction and the directions are shown in Fig. 1. The Heisenberg coupling is assumed to be antiferromagnetic ($J > 0$). The DM vector is taken to be perpendicular to the plane of the lattice as shown in the figure with constant magnitude D. The planar component of the DM vector can be taken care of by rotating the spins appropriately as long as the planar component is small [18]. Introduction of the DM interaction reduces the global spin rotation symmetry of the Heisenberg Hamiltonian from SU(2) to U(1). However, the wallpaper group remains $P6m$.

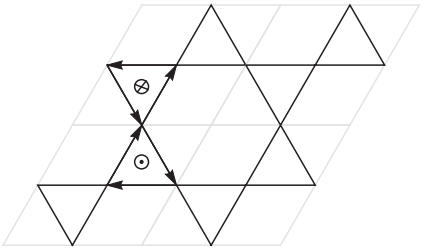

FIG. 1. Bond directions for Dzyaloshinskii-Moriya interaction where the DM vector $\vec{D}$ (shown at the center of the triangle) is staggered between up-to-down triangles.

It is expected that the DM interaction will induce long-range order and hence using the SBMFT approach is appropriate since it elegantly treats both ordered and spin liquid phases. In Schwinger boson representation the spin operators are mapped to the bosonic operators as follows:

$$S_i^\alpha = \frac{1}{2}\begin{pmatrix} a_i^\dagger & b_i^\dagger \end{pmatrix}\sigma^\alpha \begin{pmatrix} a_i \\ b_i \end{pmatrix}, \tag{2}$$

where i is the site index and $\alpha = x,y,z$. σ^α are the Pauli matrices. This mapping is faithful only when the number of bosons is equal to $2S$, that is, $(a_i^\dagger a_i + b_i^\dagger b_i) = 2S$. This constraint, in principle, must be satisfied at each site. However, it is interesting to study the properties of the bosonic system by implementing this constraint on an average basis by treating $2S$ as a parameter. Let $\kappa = \langle n_i \rangle /2$ be the boson density per flavor. The spin wave function is then obtained by applying the appropriate projection operator.

We define bond creation operators as $\hat{A}_{ij}^\dagger = \frac{1}{2}(e^{i\theta_{ij}} a_i^\dagger b_j^\dagger - e^{-i\theta_{ij}} b_i^\dagger a_j^\dagger)$ and $\hat{B}_{ij}^\dagger = \frac{1}{2}(a_i a_j^\dagger + b_i b_j^\dagger)$ with $\theta_{ij} = D_{ij}/J$. The operator $A_{ij}^\dagger$ creates a mixture of a singlet and a triplet on the bond, while $B_{ij}^\dagger$ represents coherent hopping of the bosons between the sites. These definitions are slightly different from those used by Manuel *et al.* [26]. We can rewrite the Hamiltonian in terms of these bond operators with an approximation that D/J is very small as

$$H = \sum_{\langle ij \rangle} J[: \hat{B}_{ij}^\dagger \hat{B}_{ij} : -\hat{A}_{ij}^\dagger \hat{A}_{ij}], \tag{3}$$

where :: means normal order. We decouple the quartic term by introducing mean fields $\mathcal{A}_{ij} = \langle \hat{A}_{ij} \rangle$ and $\mathcal{B}_{ij} = \langle \hat{B}_{ij} \rangle$. Then the mean-field Hamiltonian is given by

$$H_{\mathrm{MF}} = \sum_{\langle ij \rangle} J[\mathcal{B}_{ij} \hat{B}_{ij}^\dagger - \mathcal{A}_{ij} \hat{A}_{ij}^\dagger] + \mathrm{H.c.} - \sum_i \lambda_i \hat{n}_i + \epsilon_0, \tag{4}$$

where $\epsilon_0 = \sum_{\langle ij \rangle} J(\mathcal{A}_{ij}|^2 - |\mathcal{B}_{ij}|^2) + 2S\sum_i \lambda_i$. The Lagrange multiplier λ_i has been added to constrain the mean boson number at each site.

The projective symmetry group (PSG) analysis of $\mathbb{Z}_2$ spin liquids on kagome lattice was carried out by Wang and Vishwanath and they have shown that there are only four symmetric *Ansätze* possible [27]. They have labeled these *Ansätze* as $(0,0),(\pi,0),(0,\pi)$, and (π,π), based on the fluxes through the hexagon and the rhombus. These *Ansätze* respect time-reversal symmetry and lead to planar long-range order. However, Messio *et al.* have shown that ground state of the Heisenberg antiferromagnet on the kagome lattice is possibly a chiral spin liquid which is termed as *cuboc1* [23]. A systematic enumeration of *weakly symmetric* spin liquids shows that there are 20 families of spin liquid *Ansätze* on kagome lattice [28]. We restrict our choices to the four symmetric spin liquids, since DM interaction prefers planar LRO and cuboc1 spin liquid since it is energetically most favorable in the absence of DM interaction. In all *Ansätze*, the magnitudes of $\mathcal{A}_{ij}$ and $\mathcal{B}_{ij}$ are same on all bonds, that is, $|\mathcal{A}_{ij}| = \mathcal{A}$ and $|\mathcal{B}_{ij}| = \mathcal{B}$. $\mathcal{A}$ and $\mathcal{B}$ are complex numbers and their phases are summarized in the caption of Fig. 2 below. It is also assumed that the Lagrange multiplier is independent of sites and is equal to λ. Using Fourier transformation, the Hamiltonian can be written as

$$H_{\mathrm{MF}} = \sum_q \phi_q^\dagger N_q \phi_q + N[\lambda(2S+1) + 2(\mathcal{A}^2 - \mathcal{B}^2)], \tag{5}$$

where N is the number of sites and $\phi_q^\dagger = [a_{1q}^\dagger, \ldots\ldots a_{mq}^\dagger, b_{1,-q}, \ldots\ldots b_{m,-q}]$. The first index μ in $a_{\mu q}$ and $b_{\mu q}$ is the sublattice index. μ can have values 1 to m, where m is the number of sites per unit cell [$m = 3$ for the $(0,0),(\pi,0)$ *Ansätze* and $m = 6$ for *cuboc1 Ansatz*] and N_q is a $2m \times 2m$ matrix.

This N_q matrix can be diagonalized by Bogoliubov transformation $\phi_q = M_q \xi_q$, where $\xi_q^\dagger = [\alpha_{1q}^\dagger, \ldots\ldots \alpha_{mq}^\dagger, \beta_{1,-q}, \ldots\ldots \beta_{m,-q}]$. The transformation matrix must satisfy $M_q \tau M_q^\dagger = \tau$, where $\tau = \sigma_3 \otimes I_m$. We must find M_q such that $M_q^\dagger N_q M_q = \Omega_q$, where

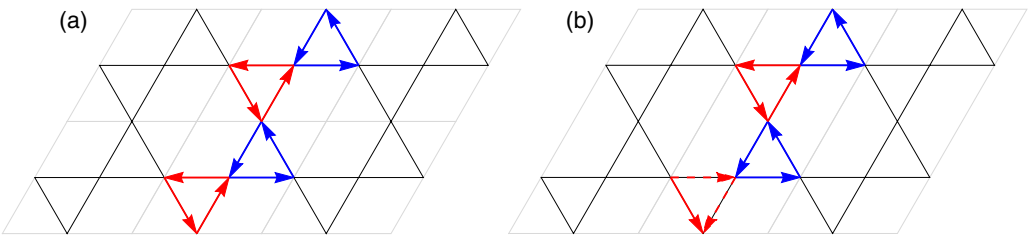

FIG. 2. Gray lines mark the three-site unit cell for the $(0,0),(\pi,0)$ *Ansatz* in (a) and the six-site unit cell for the *cuboc1 Ansatz* in (b). The mean fields are defined as $\langle \mathcal{A}_{ij} \rangle = |\mathcal{A}|e^{i\phi_\mathcal{A}}$ and $\langle \mathcal{B}_{ij} \rangle = |\mathcal{B}|e^{i\phi_\mathcal{B}}$. In (a), for the $(0,0)$ *Ansatz* $\phi_\mathcal{A} = 0$ for both the red (down) triangles and blue (up) triangles. For the $(\pi,0)$ *Ansatz* $\phi_\mathcal{A} = 0$ for the red triangles and $\phi_\mathcal{A} = \pi$ for the blue triangles. For both the *Ansätze* $\phi_\mathcal{B} = \pi$ for all bonds. In (b), for the *cuboc*1 *Ansatz*, $(\phi_A,\phi_B) = (\phi,\pi)$ for the blue triangles where ϕ is arbitrary. For red triangles, for solid lines $(\phi_A,\phi_B) = (0,\pi)$, and for dashed lines $(\phi_A,\phi_B) = (\pi,0)$.

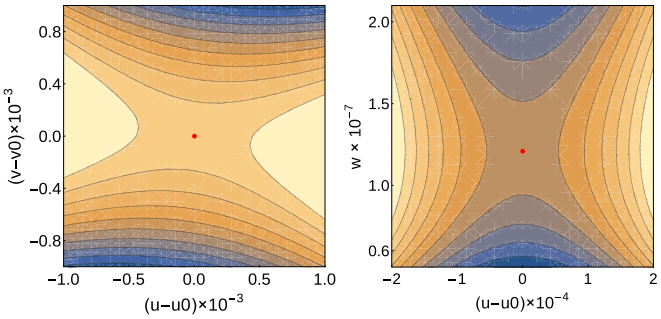

FIG. 3. Optimum points $(u0, v0, w0)$ in the rotated frame (u, v, w) for *Ansatz* $(\pi,0)$ at $\kappa = 0.366$ and $\theta = 0.21$.

$\Omega_q = \text{diag}(\omega^{\alpha}_{\mu q}.....,\omega^{\beta}_{\mu,-q})$. The form of the M_q matrix is given by $M_q = \left[\begin{smallmatrix} U_q & X_q \\ V_q & Y_q \end{smallmatrix}\right]$, where U_q, V_q, X_q, and Y_q are the $m \times m$ matrix.

The diagonalized Hamiltonian is given by

$$H_{\text{MF}} = \sum_q \sum_\mu \left(\omega^{\alpha}_{\mu q}\alpha^{\dagger}_{\mu q}\alpha_{\mu q} + \omega^{\beta}_{\mu q}\beta_{\mu q}\beta^{\dagger}_{\mu q}\right) + N[\lambda(2S+1) + 2(\mathcal{A}^2 - \mathcal{B}^2)], \tag{6}$$

where $\omega^{\alpha}_{\mu q}$ and $\omega^{\beta}_{\mu q}$ are the excitation energies of the $2m$ spinon modes. Note that for the chiral *Ansatz* $\omega^{\alpha}_{\mu q} \neq \omega^{\beta}_{\mu q}$. The ground-state energy is given by

$$E = \sum_{q,\mu} \omega^{\beta}_{\mu q} + N[\lambda(2S+1) + 2(\mathcal{A}^2 - \mathcal{B}^2)]. \tag{7}$$

The Bogoliubov matrix is computed using the procedure outlined in Ref. [29]. The mean-field parameters $\mathcal{A}, \mathcal{B}, \lambda$, and ϕ are found by extremizing the ground-state energy E. The positive definiteness of the Hamiltonian puts several conditions on the domain of these parameters. The method used for searching the saddle points is outlined in the next section. The complex link variables $\mathcal{A}_{ij}$ and $\mathcal{B}_{ij}$ satisfies the self-consistency equations

$$\mathcal{A}_{ij} = \langle \hat{\mathcal{A}}_{ij} \rangle \quad \& \quad \mathcal{B}_{ij} = \langle \hat{\mathcal{B}}_{ij} \rangle, \tag{8}$$

which are equivalent to extremization of free energy as

$$\frac{\partial E}{\partial \mathcal{A}} = \frac{\partial E}{\partial \mathcal{B}} = \frac{\partial E}{\partial \phi} = \frac{\partial E}{\partial \lambda} = 0. \tag{9}$$

III. NUMERICAL SEARCH FOR SADDLE POINTS

The bosonic mean-field Hamiltonian is diagonalizable if N_q is positive definite for all q. We begin the search by finding the valid domain in parameter space $\{\mathcal{A}, \mathcal{B}, \lambda\}$ where this condition is true. The gapless LRO phases emerge as the corresponding saddle point approaches the boundaries, thus closing the gap in the spinon spectrum. These points are difficult to find, since the eigen values of the Hessian have drastically varrying magnitude at the saddle point (see Fig. 3). As an example we have given the Hessian matrix of *Ansatz* $(\pi,0)$ at $S = 0.366$, $\theta = 0.21$, and $N = 20$:

$$h = \begin{pmatrix} 0.9230 & -0.5794 & -1.0186 \\ -0.5794 & -3.6344 & -0.3558 \\ -1.0186 & -0.3558 & -9.9997 \times 10^{11} \end{pmatrix}.$$

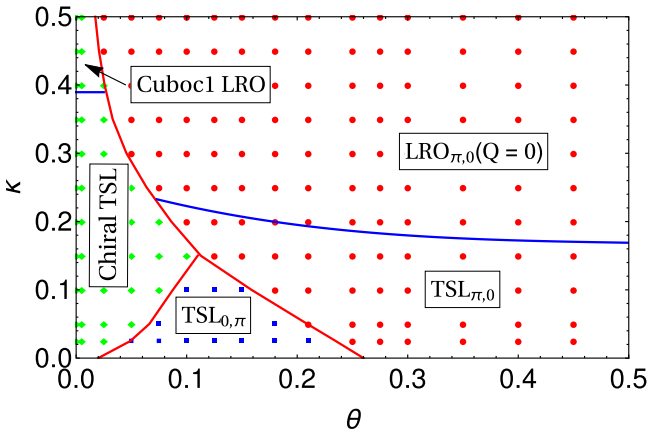

FIG. 4. Ground-state phase diagram at $T = 0$. In the phase diagram second-ordered phase transitions are shown in blue and the first-ordered transitions by red lines.

The eigenvalues of h are given by $\{-9.999\,7 \times 10^{11}, -3.706\,9, 0.995\,5\}$. Thus in LRO phases, we rotate coordinate axes which are nearly parallel to the eigenvectors of the Hessian, two of which are parallel to the boundary surface. The main hurdle in this procedure is finding boundary surfaces. However, these can be guessed by examining the classical orders. Thus analyzing eigenvalues of N_q at a few high-symmetry points in the reciprocal lattice is enough. For the (0,0) *Ansatz*, the boundary plane is given by

$$\sqrt{3}|\cos\theta|\mathcal{A} + \mathcal{B} + \lambda = 0. \tag{10}$$

The boundary surfaces in the *cuboc1* state are not planar but then it is still possible to search for a saddle point along the surfaces and then in the perpendicular direction. In this way we have been able to achieve much better accuracy where the sum of squares of gradients is of the order of 10^{-14}.

IV. PROPERTIES AND THE PHASE DIAGRAM

We have computed energies for various values of κ (0 to 0.5) and θ (0 to $\pi/6$) for all *Ansätze*. Based on the energy and the gap in the spinon spectrum, our proposed ground-state phase diagram is shown in Fig. 4. As expected, for low values of κ and also small strengths of DM interaction, the phases are gapped topological spin liquids (TSLs). For $\theta \lesssim 0.5$, the gap in the spinon spectrum closes at about $\kappa = 0.39$, indicating a second-ordered transition from gapped liquid phase to gapless cuboctahedral LRO. For large strength of DM interaction, that is, for $\theta > 0.2$, the system enters $\mathbf{Q} = 0$ LRO phase at $\theta \gtrsim 0.2$. Figure 5 shows that the gap closes at $\kappa = 0.18$ for $\theta = 0.3$.

To illustrate the nature of various phases we also have calculated the static spin structure factor

$$S^{\alpha\alpha}(\mathbf{Q}) = \frac{3}{4N}\sum_{i,j} q^{i\mathbf{Q}\cdot(\mathbf{R}_i - \mathbf{R}_j)}\langle 0|S^{\alpha}_i S^{\alpha}_j|0\rangle,$$

where $\alpha = x, y, z$, $\mathbf{R}_i$, and $\mathbf{R}_j$ are the positions of the site i and j. Due to DM interaction, the global spin rotation symmetry is reduced to U(1), and hence one must calculate both S^{xx} and

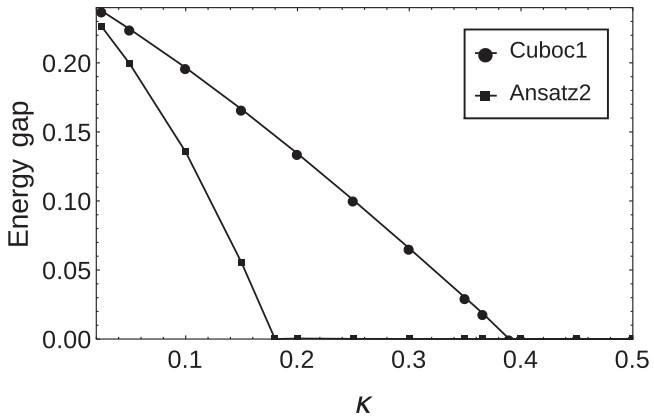

FIG. 5. Variation of energy gap with κ for the *cuboc1 Ansatz* at $\theta = 0$ and the $(\pi,0)$ *Ansatz* at $\theta = 0.30$.

S^{zz}. The expressions for the structure factor in terms of the Bogoliubov matrices are given in the Appendix.

A. Spin liquid phases

The phases of the isotropic Heisenberg model ($\theta = 0$) have been studied by Messio *et al.* [23] and our results match with them. For $\kappa > 0.39$, the spinon spectrum is gapless at $\mathbf{Q} = \frac{3}{2}\mathbf{K}$. At $\kappa \leqslant 0.39$, the gap opens up and the system enters a chiral spin liquid phase and remains in this phase down to $\kappa = 0$. Figure 5 shows the variation of energy gap as a function of κ. However, it is interesting to note that the short-range correlations are cuboctahedral near the phase transition, but as κ is decreased the peak in static structure factor becomes broad but also shifts toward the $\mathbf{K}$ point [Fig. 6(a)] before flattening out at $\kappa = 0.1$. Thus the short-range correlations become more like $\sqrt{3} \times \sqrt{3}$ type as κ is decreased, which is consistent with the $q_1 = -q_2$ spin liquid state obtained by Huh *et al.* [22].

For small values of boson density, $\kappa(< 0.15)$, the quantum fluctuations prevent any sort of long-range order in the system, even in the presence of strong DM interaction. For very small values of θ, the system persists in *cuboc1* spin liquid phase before making a first-order transition to $(0,\pi)$ spin liquid phase. In this phase, the static structure factor again shows a very broad peak at the $\mathbf{K}$ point. As the strength of the DM interaction is further increased, the system enters $(\pi,0)$ spin liquid phase with the short-range correlations of type $\boldsymbol{Q} = 0$, showing a broad peak in spin structure factor at point $\mathbf{M}_e$. Comparing with the phase diagram obtained by Messio, this transition occurs at much smaller values of DM interaction. This indicates the inclusion of $\mathcal{B}$ fields helps stabilize the $(\pi,0)$ spin liquid against the $(0,\pi)$ phase.

B. Néel ordered phases

For very small values of DM interaction and $\kappa > 0.39$, all three *Ansätze* $(0,0)$, $(0,\pi)$, and *cuboc1* are all in gapless phases corresponding to the classical orders $\sqrt{3} \times \sqrt{3}$, $\boldsymbol{Q} = 0$, and cuboctahedral, respectively [30]. However, the lowest energy is *cuboc1 Ansatz*. In this phase, the soft modes in the spinon spectrum are at $\frac{3}{4}\mathbf{K}$ points in the extended Brillouin zone. Even though the *Ansatz* is still symmetric, the mechanism of symmetry breaking leading to emergence of long-range order through Bose condensation is well understood and is described in Sachdev [31] and Messio *et al.* [28]. The spin structure factor in this phase shows strong peaks at the $\frac{3}{2}\mathbf{K}$ point, which confirms the *cuboc1* LRO phase [Fig. 6(c)]. At $\kappa = \frac{1}{2}$, the system is in *cuboc1* LRO phase for $\theta < 0.017\,3$ and then enters the $\boldsymbol{Q} = 0$ phase with a first-order phase transition. This width of *cuboc1* LRO decreases as $\kappa \to \infty$, where even infinitesimal DM interaction immediately orders the system in planar configuration.

For $\theta > 0.1$, the $(\pi,0)$ spin liquid shares a phase boundary with the $\mathbf{Q} = 0$ phase, which is favored by DM interaction. Across this boundary, the gap closes at $Q = 0$. The signature sharp peaks in static structure factor at the $\mathbf{M}_e$ point. The condensate fraction x_0 in soft mode at q_0 can be computed using

$$\frac{1}{2S}\sum_i \langle n_i \rangle = x_{q_0} N + \sum_{\substack{j,i\neq i_0 \\ q\neq q_0}} \frac{|V_{ij}(q)|^2}{S}.$$

Figure 7(a) shows the emergence of the condensate fraction as a function of θ along the $\kappa = 0.366$ horizontal line in the phase diagram. The condensate fraction is zero in the *cuboc1 Ansatz* and becomes nonzero for the $(\pi,0)$ *Ansatz* via first-order phase transition at $\theta \approx 0.03$. In Fig. 7(b), for $\kappa = 0.2$ the second-order phase transition occurs near $\theta = 0.15$ for the $(\pi,0)$ *Ansatz*.

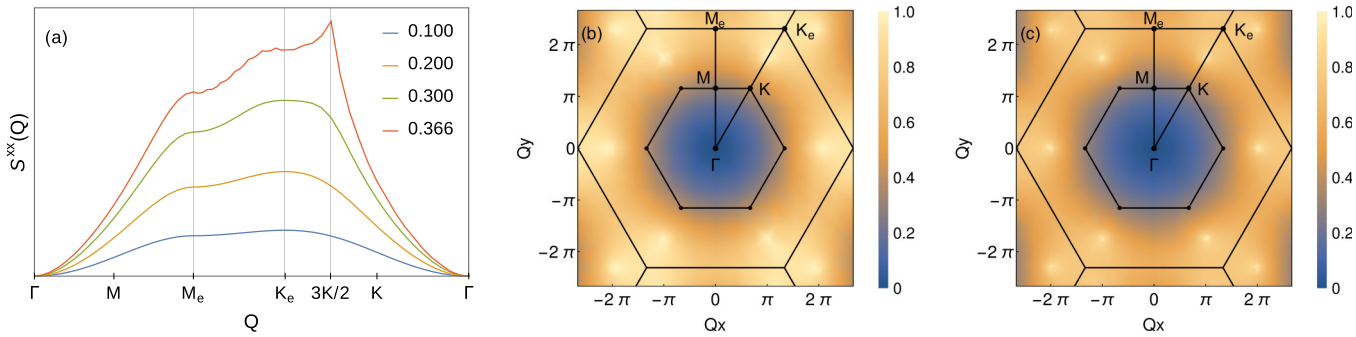

FIG. 6. (a) XX component of static structure factor along the high-symmetry line $\Gamma - M_e - K_e - \Gamma$ for the *cuboc1 Ansatz* for different values of κ at $\theta = 0$. The XX component of the static structure factor for the *cuboc1 Ansatz* at (b) $\kappa = 0.366$ and $\theta = 0$, and (c) $\kappa = 0.5$ and $\theta = 0$.

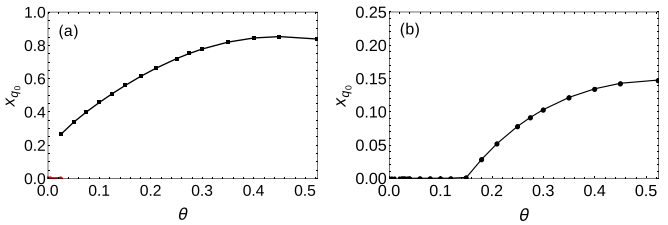

FIG. 7. Condensate fraction x_{q_0} as a function of θ (a) in the ground state at $\kappa = 0.366$ where the red points show the *cuboc1 Ansatz* and the black points show the $(\pi,0)$ *Ansatz* and (b) for the $(\pi,0)$ *Ansatz* at $\kappa = 0.2$.

C. Discussion

The ground-state phase diagram obtained here is qualitatively similar to that of Messio *et al.* [21] except that the *cuboc1 Ansatz* replaces the (0,0) *Ansatz* in the phase diagram. The results obtained at $\kappa = 1/2$, however, are not in agreement with earlier studies for the spin-1/2 system [18,22,32], which predict a moment-free phase for small values of θ and a second-ordered phase transition to $\mathbf{Q} = 0$ phase. However, the nature of the short-range correlations in the liquid phase is unclear. Cépas *et al.* [18] argue that the short-range correlations are of type $\mathbf{Q} = 0$, whereas Huh *et al.* [22] showed it to be of $\sqrt{3} \times \sqrt{3}$ type. However, Messio *et al.* [23] have argued that, in SBMFT, since the $n_i = 2S$ constraint is implemented only in an average sense, the spin-1/2 system may not be correctly represented by $\kappa = 1/2$. Due to the fluctuations in n_i, the $\langle \boldsymbol{S}_i^2 \rangle$ is overestimated to be $\frac{3}{2}S(S+1)$ at $\theta = 0$. If we treat $\langle \boldsymbol{S}_i^2 \rangle$ to be a good quantum number, then the spin-1/2 system is approximated by the bosonic system at $\kappa = 0.366$. At this value of κ, our proposal shows that the system is a $\mathbb{Z}_2$ chiral spin liquid until $\theta < 0.03$, with short-range correlations of the cuboctahedral kind. For $\theta > 0.03$, the DM interaction forces the spins to be in planar arrangement with $\boldsymbol{Q} = 0$ long-range order.

It is also possible that the best representation may be at smaller values of κ, where we have noted that the short-range correlations tend to be more like $\sqrt{3} \times \sqrt{3}$ type, as argued by Messio *et al.* Even though at $\kappa = 0.366$ it shows a first-order transition from spin liquid to $\mathbf{Q} = 0$ LRO, it may not be adequate in reconciling with the experimental results. The strength of the DM interaction is estimated to be $0.08J$ in $ZnCu_3(OH)_6Cl_3$. This compound does not exhibit freezing of magnetic moments to very low temperatures [12]. In the present mean-field theory, at $\kappa = 0.366$, the critical $D_c = 0.03J$. The optimized value of mean-field parameters and energy for $\kappa = 0.366$ is as given in Table I below. (Also, please see the *"Note added"* at the end of this article.)

TABLE I. Optimized values and energies for different *Ansätze*.

Ansatz	θ	$\mathcal{A}$	$\mathcal{B}$	λ	ϕ	Energy
cuboc1	0	0.4036	0.1185	−0.5803	1.9847	−0.2976
$(\pi,0)$	0.21	0.4226	0.1340	−0.6700		−0.3213

V. DYNAMICAL SPIN STRUCTURE FACTOR

Since in neutron scattering experiments the inelastic neutron scattering cross section is proportional to the dynamical spin structure factor, we have calculated the dynamical spin structure factor defined by

$$S^{\alpha\alpha}(\mathbf{Q},\omega) = \int_{-\infty}^{\infty} \langle 0|S^{\alpha}_{-\mathbf{Q}}(t) S^{\alpha}_{\mathbf{Q}}(0)|0\rangle e^{i\omega t} dt, \qquad (11)$$

where $\alpha = x,y,z$ and $|0\rangle$ is the ground state of the system. The expressions for the ZZ and XX components of the dynamical structure factor in terms of Bogoliubov matrices are given in the Appendix. For numerical purposes, the δ function is approximated by a Lorentzian function. The results are qualitatively similar to the results obtained by Messio *et al.* [21].

In Fig. 8 we illustrate the evolution of the dynamical structure factor across the phase transition from spin liquid to LRO phase for $\kappa = 0.366$. The dynamical structure factor is shown along the high-symmetry line $\Gamma - \mathbf{M}_e - \mathbf{K}_e - \Gamma$. The dynamical structure factor of *cuboc1 Ansatz* at $\theta = 0$ in Fig. 8(a) shows a sharp onset of spinon continuum at $\frac{3}{2}\mathbf{K}$ with a very small gap. This is due to the proximity of the critical point at $\kappa = 0.39$ beyond which there is *cuboc1* long-range order.

Since the DM interaction reduces the global spin rotation symmetry from SU(2) to U(1), there is a notable difference between the XX and ZZ components of the dynamical structure factor. In Figs. 8(b) and 8(c), we show the dynamical structure

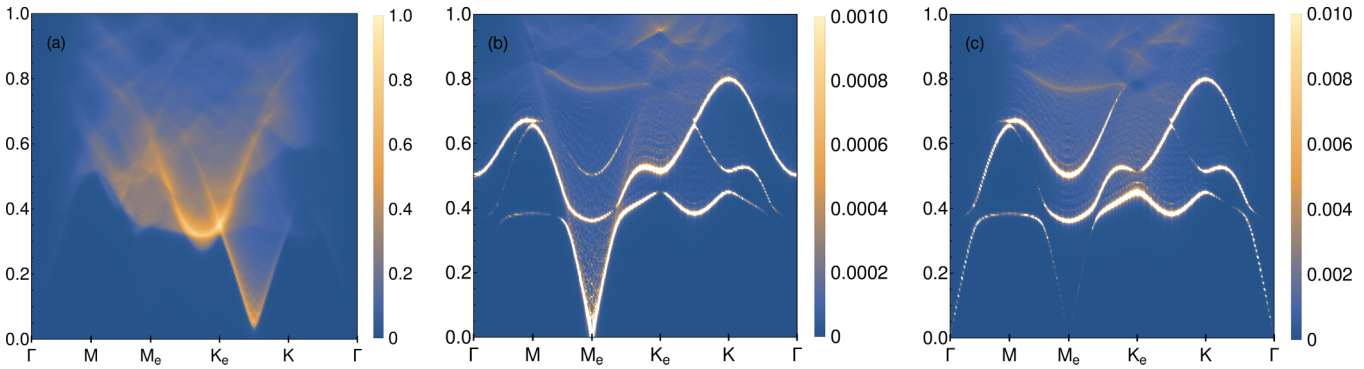

FIG. 8. XX component of the dynamical structure factor for (a) the *cuboc*1 *Ansatz* at $\kappa = 0.366$ and $\theta = 0$, (b) the $(\pi,0)$ *Ansatz* at $\kappa = 0.366$ with $\theta = 0.21$, and (c) the ZZ component of the dynamical structure factor for the $(\pi,0)$ *Ansatz* at $\kappa = 0.366$ and $\theta = 0.21$. In the LRO phase we chose the scale to be very small such that the spinon continuum is visible.

factor of the *Ansatz* $(0,\pi)$ at $\theta = 0.21$, which is the $\mathbf{Q} = 0$ LRO phase.

In the XX component of the dynamical structure factor, the magnon branches are quite strong, and in the density plot it is visible as three lines of bright dots corresponding to three magnon branches. These magnon branches are obtained by considering the pair of spinons, one in the soft modes and other one from the excited state. The elastic peak (along $\omega = 0$ line) appears with largest intensity at point $\mathbf{M}_e$, which is the Γ point of the next Wigner- Seitz cell.

In the ZZ component of dynamical structure factor the magnon branches are of very low intensity and are suppressed, as the spins are forced to lie in the XY plane due to the DM interaction.

VI. CONCLUSION

We have computed the ground-state phase diagram of the Heisenberg kagome antiferromagnet with DM interaction using the SBMFT approach. We have included the time-reversal symmetry-breaking chiral *Ansatz* proposed by Messio *et al.* [23] and also considered the hopping mean field $\mathcal{B}$. For large S, even with small DM interaction, the spins are forced to lie in the plane which leads to $\mathbf{Q} = 0$ long range order. For small S, the quantum fluctuations induce a series of spin liquid phases with increasing DM interaction. In this region, the inclusion of the hopping field seems to stabilize the $(\pi,0)$ spin liquid phase over the $(0,\pi)$ spin liquid.

Since the constraint of boson density is implemented strictly, $\langle \mathbf{S}_i^2 \rangle = \frac{1}{2}$ at $\kappa = 0.366$ due to the fluctuations in boson density. We find that at $\kappa = 0.366$, the model shows a first-ordered phase transition from chiral *cuboc1* spin liquid to $\mathbf{Q} = 0$ Néel phase at $D = 0.03J$. Even though this result is qualitatively in agreement with other studies, it is not adequate in explaining the moment-free phase of herbertsmithite [12], since the estimated DM strength is $0.08J$. Probably, one may need to consider even smaller values of κ to obtain better numerical agreement with other studies and experiment. We, have also calculated a static and dynamical structure factor at the representative $\kappa = 0.366$ point.

Note added. After we submitted this manuscript, Messio *et al.* [33] published an article in which they pointed out that one more ansatz results in a stable phase. This article demonstrates that an additional phase [termed as $A_4(0,1)$] is stable in small κ and in the small θ region of the phase diagram sandwiched between the chiral spin liquid and $TSL_{0,\pi}$ phases.

APPENDIX

1. Static spin structure factor

The expression for the XX component of the static spin structure factor is given by

$$\begin{aligned} S^{xx}(\mathbf{Q}) = \frac{3}{16N}\sum_{q,\mu\nu}\big[\big[X^*_{\mathbf{Q}+q}Y^T_{\mathbf{Q}+q}\big]_{\mu\nu}\big[Y^*_{-q}X^T_{-q}\big]_{\mu\nu} \\ + \big[X^*_{\mathbf{Q}+q}X^T_{\mathbf{Q}+q}\big]_{\mu\nu}\big[Y^*_{-q}Y^T_{-q}\big]_{\mu\nu} \\ + [V_qU_q^\dagger]_{\mu\nu}[U_{-\mathbf{Q}-q}V^\dagger_{-\mathbf{Q}-q}]_{\mu\nu} \\ + [V_{-\mathbf{Q}-q}V^\dagger_{-\mathbf{Q}-q}]_{\mu\nu}[U_qU_q^\dagger]_{\mu\nu}\big]. \end{aligned} \tag{A1}$$

The ZZ component of the structure factor has the form

$$\begin{aligned} S^{zz}(\mathbf{Q}) = \frac{3}{16N}\sum_{q,\mu,\nu}\big[\big[X^*_{\mathbf{Q}+q}X^T_{\mathbf{Q}+q}\big]_{\mu\nu}[U_qU_q^\dagger]_{\mu\nu}\big] \\ + [V_{-\mathbf{Q}-q}V^\dagger_{-\mathbf{Q}-q}]_{\mu\nu}\big[X^*_{-q}X^T_{-q}\big]_{\mu\nu} \\ - \big[X^*_{\mathbf{Q}+q}Y^T_{\mathbf{Q}+q}\big]_{\mu\nu}[U_qV_q^\dagger]_{\mu\nu} \\ - [V_{-\mathbf{Q}-q}U^\dagger_{-\mathbf{Q}-q}]_{\mu\nu}\big[Y^*_{-q}X^T_{-q}\big]_{\mu\nu}. \end{aligned} \tag{A2}$$

2. Dynamical spin structure factor

The expression for the XX component of the dynamical spin structure factor is given by

$$\begin{aligned} S^{xx}(\mathbf{Q},\omega) = 2\pi\sum_q\sum_{\mu\nu}\big[|[U_q^\dagger V^*_{-q-\mathbf{Q}}]_{\mu\nu} + [U^\dagger_{-q-\mathbf{Q}}V^*_q]_{\nu\mu}|^2 \\ + \big|\big[Y^T_{-q}X_{q+\mathbf{Q}}\big]_{\mu\nu} + \big[Y^T_{\mathbf{Q}+q}X_{-q}\big]_{\nu\mu}\big|^2\big] \\ \times\delta(\omega-\omega_p), \end{aligned} \tag{A3}$$

where μ,ν are the sublattice index. The expression for the ZZ component of dynamical spin structure factor reduces to

$$\begin{aligned} S^{zz}(\mathbf{Q},\omega) = 2\pi\sum_q\sum_{\mu\nu}|[U_q^\dagger X_{\mathbf{Q}+q}]_{\mu\nu} - [V_q^\dagger Y_{\mathbf{Q}+q}]_{\mu\nu}|^2 \\ \times\delta(\omega-\omega_p), \end{aligned} \tag{A4}$$

where $\omega_p = \omega_q + \omega_{-\mathbf{Q}-q}$. At $\mathbf{Q} = 0$ the zz component will straightaway give zero because it is just the dot product of the two columns of the M matrix (para orthogonalization), consistent with the figure.

[1] P. Anderson, Mater. Res. Bull. **8**, 153 (1973).
[2] C. Lhuillier and G. Misguich, in *Introduction to Frustrated Magnetism* (Springer, New York, 2011), pp. 23–41.
[3] F. Mila, Eur. J. Phys. **21**, 499 (2000).
[4] L. Balents, Nature (London) **464**, 199 (2010).
[5] L. Savary and L. Balents, Rep. Prog. Phys. **80**, 016502 (2016).
[6] P. W. Leung and V. Elser, Phys. Rev. B **47**, 5459 (1993).
[7] S. Yan, D. A. Huse, and S. R. White, Science **332**, 1173 (2011).
[8] H. C. Jiang, Z. Y. Weng, and D. N. Sheng, Phys. Rev. Lett. **101**, 117203 (2008).
[9] Y. Ran, M. Hermele, P. A. Lee, and X.-G. Wen, Phys. Rev. Lett. **98**, 117205 (2007).
[10] I. Dzialoshinskii, Sov. Phys. JETP **5**, 1259 (1957).
[11] T. Moriya, Phys. Rev. **120**, 91 (1960).
[12] J. Helton, K. Matan, M. Shores, E. Nytko, B. Bartlett, Y. Yoshida, Y. Takano, A. Suslov, Y. Qiu, J.-H. Chung *et al.*, Phys. Rev. Lett. **98**, 107204 (2007).

[13] P. A. Lee, Science **321**, 1306 (2008).
[14] B. G. Levi, Phys. Today **60**(2), 16 (2007).
[15] A. Zorko, S. Nellutla, J. van Tol, L. C. Brunel, F. Bert, F. Duc, J.-C. Trombe, M. A. De Vries, A. Harrison, and P. Mendels, Phys. Rev. Lett. **101**, 026405 (2008).
[16] M. Rigol and R. R. P. Singh, Phys. Rev. Lett. **98**, 207204 (2007).
[17] I. Rousochatzakis, S. R. Manmana, A. M. Läuchli, B. Normand, and F. Mila, Phys. Rev. B **79**, 214415 (2009).
[18] O. Cépas, C. M. Fong, P. W. Leung, and C. Lhuillier, Phys. Rev. B **78**, 140405 (2008).
[19] M. Tovar, K. S. Raman, and K. Shtengel, Phys. Rev. B **79**, 024405 (2009).
[20] M. Hermele, Y. Ran, P. A. Lee, and X.-G. Wen, Phys. Rev. B **77**, 224413 (2008).
[21] L. Messio, O. Cépas, and C. Lhuillier, Phys. Rev. B **81**, 064428 (2010).
[22] Y. Huh, L. Fritz, and S. Sachdev, Phys. Rev. B **81**, 144432 (2010).
[23] L. Messio, B. Bernu, and C. Lhuillier, Phys. Rev. Lett. **108**, 207204 (2012).
[24] A. Mezio, C. Sposetti, L. Manuel, and A. Trumper, Europhys. Lett. **94**, 47001 (2011).
[25] R. Flint and P. Coleman, Phys. Rev. B **79**, 014424 (2009).
[26] L. O. Manuel, C. J. Gazza, A. E. Trumper, and H. A. Ceccatto, Phys. Rev. B **54**, 12946 (1996).
[27] F. Wang and A. Vishwanath, Phys. Rev. B **74**, 174423 (2006).
[28] L. Messio, C. Lhuillier, and G. Misguich, Phys. Rev. B **87**, 125127 (2013).
[29] J. Colpa, Physica A (Amsterdam, Neth.) **93**, 327 (1978).
[30] L. Messio, C. Lhuillier, and G. Misguich, Phys. Rev. B **83**, 184401 (2011).
[31] S. Sachdev, Phys. Rev. B **45**, 12377 (1992).
[32] A. Laeuchli and C. Lhuillier, arXiv:0901.1065.
[33] L. Messio, S. Bieri, C. Lhuillier, and B. Bernu, arXiv:1701.01243.